

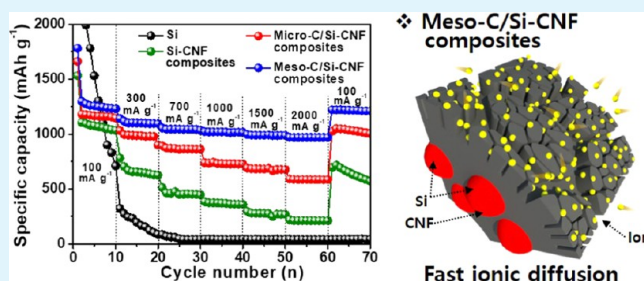
Improved Ionic Diffusion through the Mesoporous Carbon Skin on Silicon Nanoparticles Embedded in Carbon for Ultrafast Lithium Storage

Geon-Hyoung An,[†] Hyeonjin Kim,[‡] and Hyo-Jin Ahn^{*,†,‡,§}[†]Program of Materials Science & Engineering, Convergence Institute of Biomedical Engineering and Biomaterials and [‡]Department of Materials Science and Engineering, Seoul National University of Science and Technology, Seoul 01811, Korea

Supporting Information

ABSTRACT: Because of their combined effects of outstanding mechanical stability, high electrical conductivity, and high theoretical capacity, silicon (Si) nanoparticles embedded in carbon are a promising candidate as electrode material for practical utilization in Li-ion batteries (LIBs) to replace the conventional graphite. However, because of the poor ionic diffusion of electrode materials, the low-grade ultrafast cycling performance at high current densities remains a considerable challenge. In the present study, seeking to improve the ionic diffusion, we propose a novel design of mesoporous carbon skin on the Si nanoparticles embedded in carbon by hydrothermal reaction, poly(methyl methacrylate) coating process, and carbonization. The resultant electrode offers a high specific discharge capacity with excellent cycling stability (1140 mA h g⁻¹ at 100 mA g⁻¹ after 100 cycles), superb high-rate performance (969 mA h g⁻¹ at 2000 mA g⁻¹), and outstanding ultrafast cycling stability (532 mA h g⁻¹ at 2000 mA g⁻¹ after 500 cycles). The battery performances are surpassing the previously reported results for carbon and Si composite-based electrodes on LIBs. Therefore, this novel approach provides multiple benefits in terms of the effective accommodation of large volume expansions of the Si nanoparticles, a shorter Li-ion diffusion pathway, and stable electrochemical conditions from a faster ionic diffusion during cycling.

KEYWORDS: Li-ion battery, anode, ultrafast cycling, mesoporous structure, carbon, silicon



INTRODUCTION

In recent years, due to eco-friendliness without carbon dioxide emissions and low fuel prices, electric vehicles have become the next-generation transportation to replace the conventional vehicles using fossil fuels. However, electric vehicles still face critical challenges, such as low mileage (e.g., model 3, Tesla: 215 miles). Therefore, much effort has been invested to increase the mileage using diverse approaches, including decrease of car body, improvement of electric motor, and enhancement of batteries.^{1–5} Batteries, the principal power source for electric vehicles, are almost prepared using Li-ion batteries (LIBs) having a high energy density, excellent cycling stability, eco-compatibility, low memory loss, and low self-discharge rate.^{6–8} However, the improvement of the LIB capacity is very difficult due to limitations such as theoretical capacity. Therefore, we need a new way to improve the user environment of electric vehicles. In this context, the ultrafast charge ability of LIBs (called ultrafast LIBs) is a potential candidate to redeem the challenge of the short mileage. However, the low capacity of the anode electrode, which is commonly made of graphite, is a more important limitation than the cathode electrode during the ultrafast cycling with rapid volume expansion and faster ionic diffusion.^{9–11} To overcome these problems, carbon-coating engineering on the

electrode materials with thin skin has been effectively employed, therefore accepting the rapid volume expansion.^{12–15} However, despite these efforts, the anode electrode still indicates a low ultrafast cycling performance arising from its poor ionic diffusion.

In the present study, we suggest a unique nanoarchitecture of mesoporous carbon skin on silicon (Si) nanoparticles embedded in carbon nanofiber (Meso-C/Si-CNF composites), where Si has a high theoretical capacity (~4200 mA h g⁻¹) and a low electrochemical working voltage of <0.5 V.^{3,4,16} First, an extra carbon skin as the physical buffer layer was introduced on the skin of Si nanoparticles embedded in carbon nanofiber to accommodate the rapid volume expansion. In addition, the spotlight of this study is the development of a mesoporous carbon skin (pore size: >2 nm) to achieve faster ionic diffusion, which is an opener to obtain excellent ultrafast cycling performance at high current densities. Moreover, networked electrodes with a one-dimensional structure, such as CNF, can provide an effective electron transfer, leading to an improved ultrafast cycling performance.^{17,18}

Received: October 20, 2017

Accepted: January 30, 2018

Published: January 30, 2018

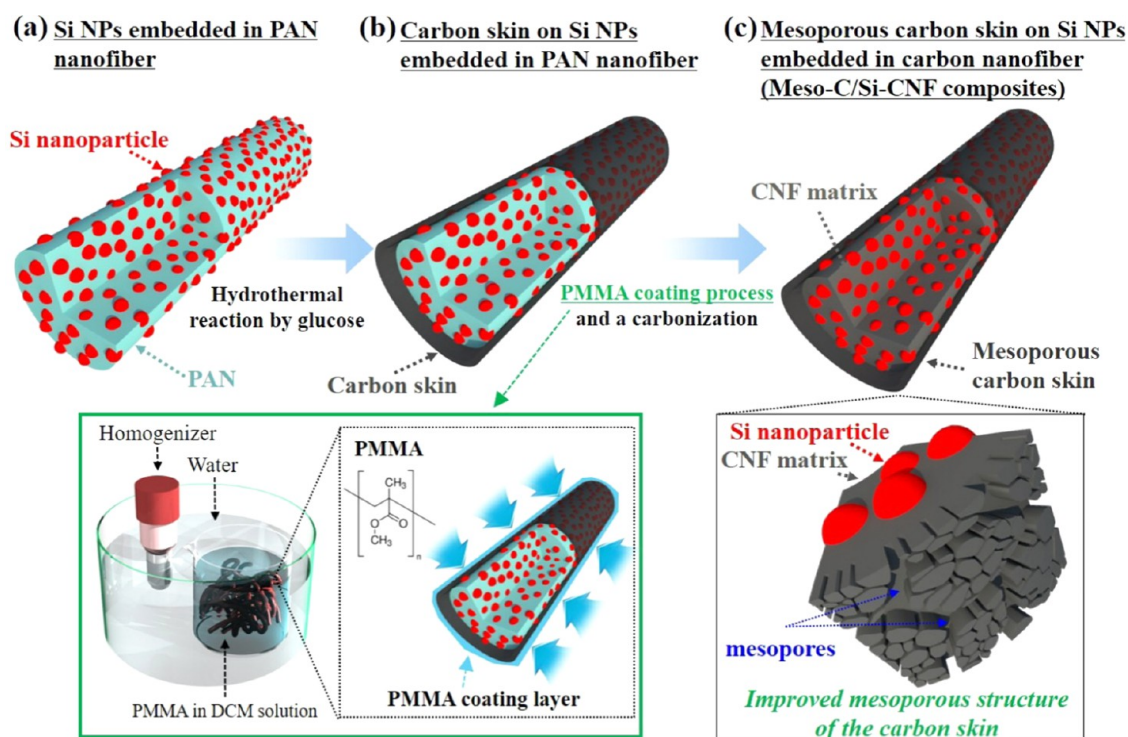


Figure 1. Schematic illustration of the synthesis process for (a) PAN nanofibers with embedded Si nanoparticles, (b) carbon skin-covered PAN nanofibers with embedded Si nanoparticles, and (c) Meso-C/Si-CNF composites.

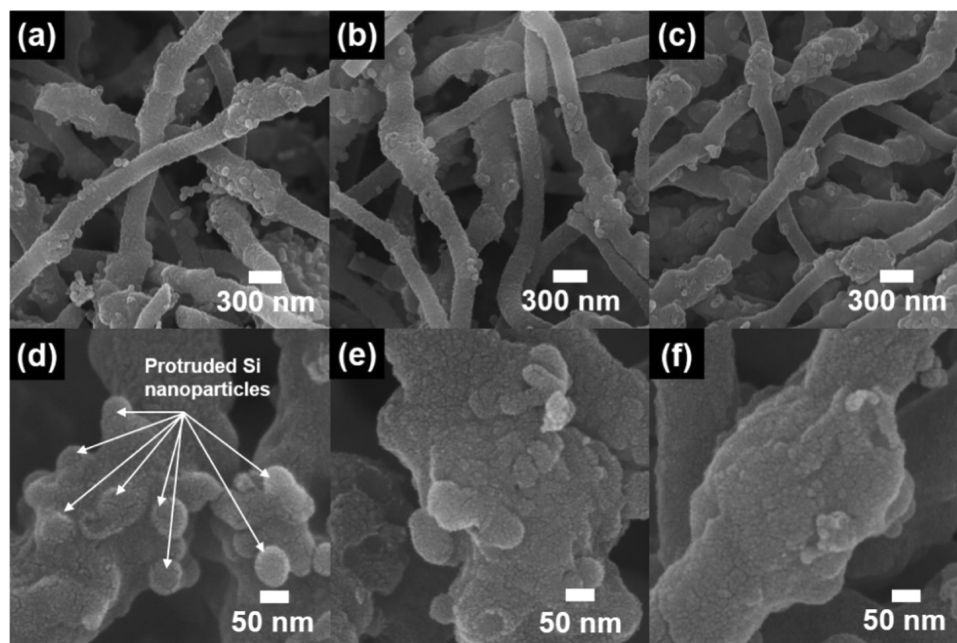


Figure 2. (a–c) Low-magnification and (d–f) high-magnification SEM images of Si-CNF composites, Micro-C/Si-CNF composites, and Meso-C/Si-CNF composites.

Therefore, the unique nanoarchitecture of Meso-C/Si-CNF composites has critical benefits, such as a carbon skin for high capacity with a superb cycling stability and a mesoporous carbon skin to permit ultrafast cycling performance. For comparison, Si nanoparticles embedded in CNF (referred to as Si-CNF composites) without the extra carbon skin on the surface and the microporous carbon skin on Si nanoparticles embedded in CNF (referred to as Micro-C/Si-CNF composites) were used.

RESULTS AND DISCUSSION

The synthesis process of the novel structure of Meso-C/Si-CNF composites via the hydrothermal reaction and the poly(methyl methacrylate) (PMMA, $M_w = \sim 120\,000$) coating process is shown in Figure 1. First, Si nanoparticles embedded in polyacrylonitrile (PAN, $M_w = 150\,000$) nanofiber (Figure 1a) were prepared by electrospinning. Next, the carbon skin on Si nanoparticles embedded in PAN nanofiber (Figure 1b) was

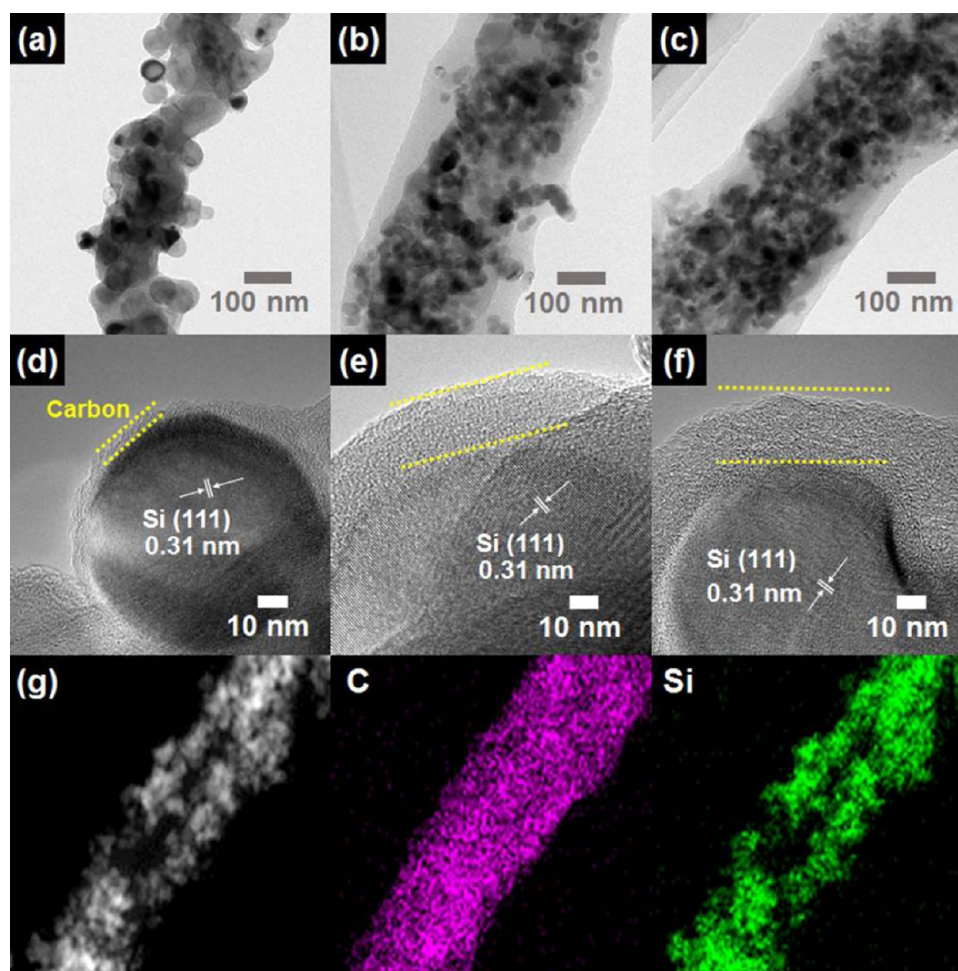


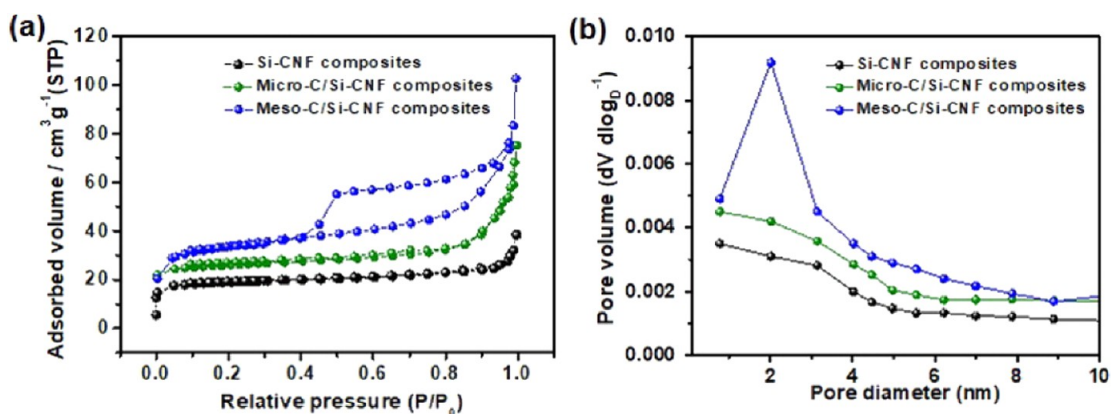
Figure 3. (a–c) Low-magnification and (d–f) high-magnification TEM images of Si-CNF composites, Micro-C/Si-CNF composites, and Meso-C/Si-CNF composites. (g) TEM–EDS spectra of Meso-C/Si-CNF composites.

fabricated using a hydrothermal reaction by glucose. Finally, the novel structure of a mesoporous carbon skin of Meso-C/Si-CNF composites (Figure 1c) was synthesized by the PMMA coating process using a homogenizer through carbonization. As PMMA plays the key role in forming the mesoporous carbon skin, PMMA resulting from the formation of the mesopore was decomposed during the carbonization process.

Figure S1 shows the scanning electron microscopy (SEM) and transmission electron microscopy (TEM, Gwangju Center, Korea Basic Science Institute) images of Si nanoparticles. The particle size distribution of pure Si nanoparticles is 20–110 nm, as shown in Figure S1c. Figure 2 shows low-magnification (Figure 2a–c) and high-magnification (Figure 2d–f) SEM images of Si-CNF composites, Micro-C/Si-CNF composites, and Meso-C/Si-CNF composites. All nanofibers had an interlinked network structure, which can be expected to achieve efficient electron transfer.^{17,18} Therefore, Si-CNF composites (Figure 2a,d) had the average diameter of 251–293 nm with protruded Si nanoparticles, implying the insufficient encapsulation of the Si nanoparticles in the CNF matrix. On the other hand, Micro-C/Si-CNF composites (Figure 2b,e) displayed the average diameter of 273–295 nm. Besides, Meso-C/Si-CNF composites (Figure 2c,f) indicated the average diameter of 272–299 nm without protruded Si nanoparticles, signifying a successful encapsulation of Si-CNF composites by the mesoporous carbon skin. Thus, the

mesoporous carbon skin of Meso-C/Si-CNF composites was developed.

To further explore the nanostructural features, TEM analysis was performed. TEM images of Si-CNF composites, Micro-C/Si-CNF composites, and Meso-C/Si-CNF composites before carbonization showed well-dispersed Si nanoparticles in the nanofiber (see Figure S2). Figure 3 shows low-magnification (Figure 3a–c) and high-magnification (Figure 3d–f) TEM images of Si-CNF composites, Micro-C/Si-CNF composites, and Meso-C/Si-CNF composites. The Si nanoparticles of Si-CNF composites (Figure 3a,d) were protruded on the surface. Therefore, a carbon layer on the surface was investigated with the thickness of 1–3 nm. Owing to the large volume expansion of Si, resulting in a quick capacity fading, the Si nanoparticles can easily crack the thin carbon layer during the lithiation/delithiation process. The Si nanoparticles of Micro-C/Si-CNF composites (Figure 3b,e) were almost wrapped using a carbon skin. Interestingly, Meso-C/Si-CNF composites (Figure 3c,f) showed the encapsulation of the Si nanoparticles by the mesoporous carbon skin with the thickness of 19–25 nm. This could physically provide a strong buffer skin. In addition, the Si nanoparticles were uniformly dispersed in the CNF matrix, leading to an improved cycling stability due to the efficient accommodation of the volume expansion of the Si nanoparticles during the lithiation/delithiation process. Furthermore, the Si nanoparticle of Meso-C/Si-CNF composites



(c) Development of the mesoporous structure

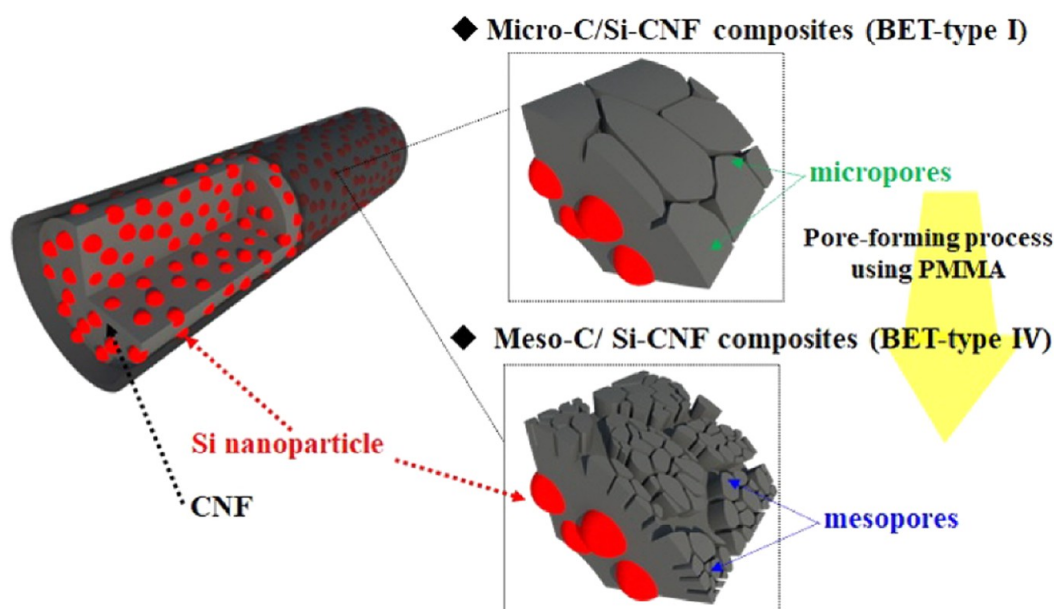


Figure 4. (a) N_2 adsorption/desorption isotherms and (b) BJH pore size distributions of Si-CNF composites, Micro-C/Si-CNF composites, and Meso-C/Si-CNF composites. (c) Schematic illustration of the pore-forming process using PMMA for Meso-C/Si-CNF composites.

Table 1. Specific Surface Area, Total Pore Volume, Average Pore Diameter, and Pore Volume Fraction of Si-CNF Composites, Micro-C/Si-CNF Composites, and Meso-C/Si-CNF Composites

samples	S_{BET} ($m^2 g^{-1}$)	total pore volume ($P/P_0 = 0.990$) ($cm^3 g^{-1}$)	average pore diameter (nm)	pore volume fraction	
				V_{micro} (%)	V_{meso} (%)
Si-CNF composites	60.1	0.02	1.3	84.8	15.2
Micro-C/Si-CNF composites	80.5	0.04	1.9	85.2	14.8
Meso-C/Si-CNF composites	123.8	0.14	4.5	52.1	47.9

(Figure 3f) had a lattice spacing of 0.31 nm, corresponding to the (111) plane of Si.^{4,19} To verify the distribution of carbon and Si, TEM–energy-dispersive spectrometry (EDS) mapping measurements were performed (Figure 3g for the results). The EDS consequence demonstrates that carbon and Si atoms are evenly dispersed, suggesting that highly dispersed Si nanoparticles are consistently wrapped by a mesoporous carbon skin.

To examine the pore structures, N_2 adsorption/desorption isotherms were investigated using the Brunauer–Emmett–Teller (BET) measurements (see Figure 4a). Isotherms of the Si-CNF and Micro-C/Si-CNF composites indicate type I features, signifying the presence of micropores (pore width, <2

nm) by the International Union of Pure and Applied Chemistry.^{20,21} The isotherm of Meso-C/Si-CNF composites shows type IV characteristics, implying the existence of mesopores (pore width, 2–50 nm) at high pressures ($P/P_0 > 0.4$).^{20,21} These results suggest that the mesoporous carbon skin is formed by the thermal decomposition of PMMA at 410 °C during carbonization, as demonstrated by the results of the differential scanning calorimetry (DSC) analysis (see Figure S3). Detailed BET consequences, including the specific surface area, average pore diameter, total pore volume, and pore volume fraction, are provided in Table 1. The specific surface area of Meso-C/Si-CNF composites ($123.8 m^2 g^{-1}$) is higher than that of Si-CNF composites ($60.1 m^2 g^{-1}$) and Micro-C/Si-

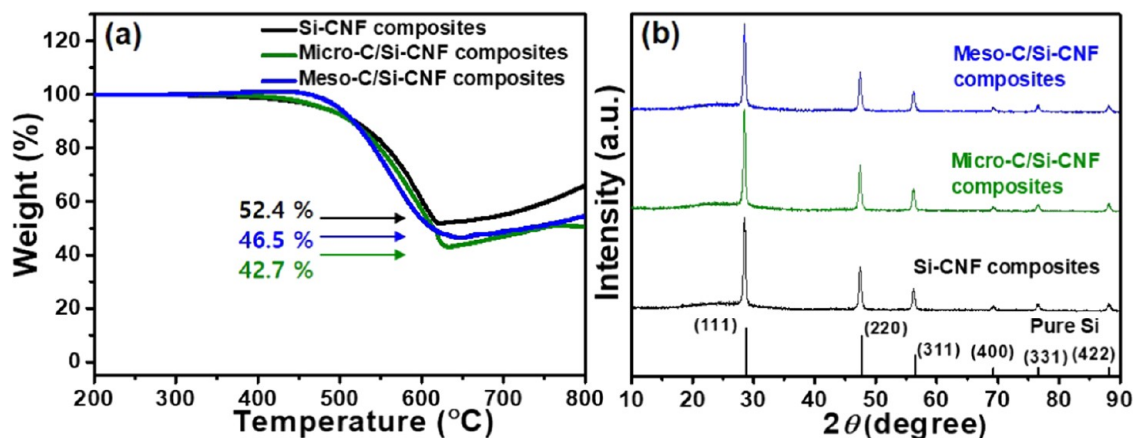


Figure 5. (a) TGA curves of Si-CNF composites, Micro-C/Si-CNF composites, and Meso-C/Si-CNF composites from 200 to 800 °C at a heating rate of 10 °C min⁻¹ in air. (b) XRD patterns of Si-CNF composites, Micro-C/Si-CNF composites, and Meso-C/Si-CNF composites.

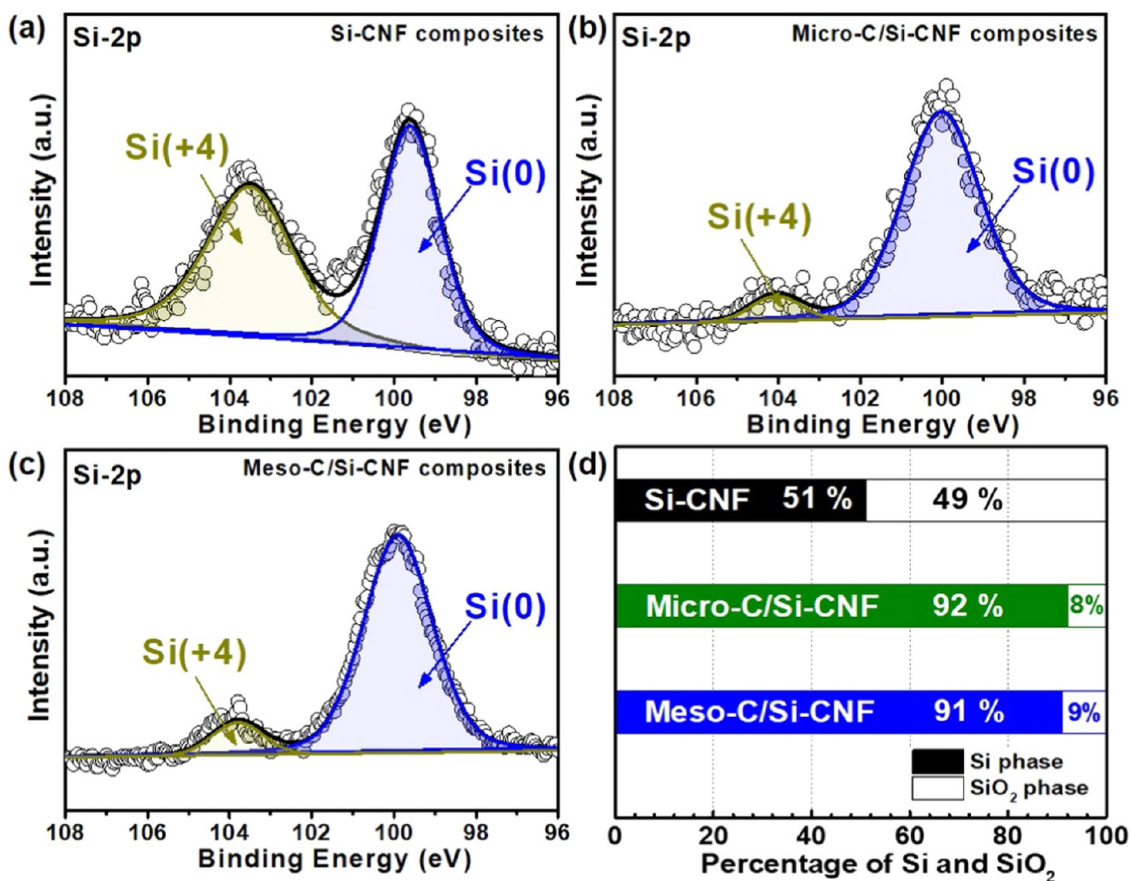


Figure 6. XPS images of Si 2p of (a) Si-CNF composites, (b) Micro-C/Si-CNF composites, and (c) Meso-C/Si-CNF composites. (d) Percentage of the Si and SiO₂ phases in the XPS images of Si 2p.

CNF composites (80.5 m² g⁻¹). Specifically, the mesopore distribution of Meso-C/Si-CNF composites was increased by the pore-forming process using PMMA. Meso-C/Si-CNF composites show the highest mesopore volume fraction of 47.9%. Thus, PMMA was decomposed during carbonization, leading to the formation of mesopores. In addition, the pore-forming process to obtain the high mesopore volume fraction was optimized using 30 wt % PMMA (see Table S1). Figure 4b displays the pore volume and pore diameter obtained using the Barrett–Joyner–Halenda (BJH) measurements. Meso-C/Si-CNF composites indicated a high pore volume in the mesopore

size range of 2–3 nm. These consequences show that Meso-C/Si-CNF composites having a high mesopore volume fraction are successfully synthesized by the pore-forming process using PMMA (see Figure 4c). The high mesopore volume fraction of Meso-C/Si-CNF composites is known to be significant for a shorter Li-ion diffusion pathway during the ultrafast lithiation/delithiation process.

To explore the content of Si-CNF composites, Micro-C/Si-CNF composites, and Meso-C/Si-CNF composites, thermogravimetric analysis (TGA) measurements were conducted, as shown in Figure 5a. For all samples, weight loss occurred

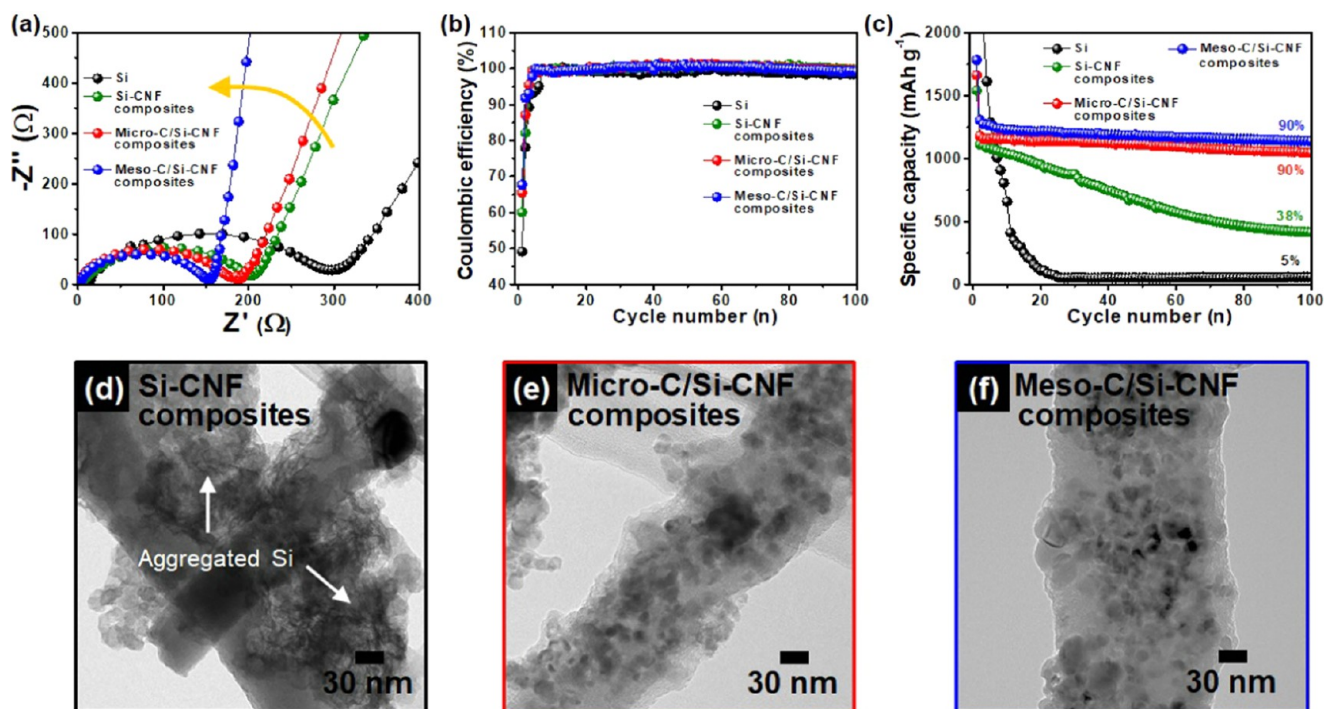


Figure 7. (a) Nyquist plots in the frequency of 10^5 – 10^{-2} Hz before charge–discharge tests; (b) Coulombic efficiencies; and (c) cycling stabilities of Si, Si-CNF composites, Micro-C/Si-CNF composites, and Meso-C/Si-CNF composites electrodes at a current density of 100 mA g^{-1} over 100 cycles. TEM images of (d) Si-CNF composites; (e) Micro-C/Si-CNF composites, and (f) Meso-C/Si-CNF composites after 100 cycles.

between 450 and 630 °C, signifying the decomposition of the CNF matrix in air. In addition, the weight loss consecutively increased with increasing temperature, implying the oxidation of the Si nanoparticles. Si-CNF composites showed a weight loss of 47.6%, indicating the existence of the Si nanoparticles in the CNFs. However, compared to Si-CNF composites, because of the formation of a carbon skin on the surface, Micro-C/Si-CNF composites revealed an increased weight loss of 57.3%. On the other hand, compared to Micro-C/Si-CNF composites, because of the developed mesoporous carbon skin, the weight loss of Meso-C/Si-CNF composites was slightly reduced to 53.5%. These results demonstrate that mesoporous carbon skin is formed by the thermal decomposition of PMMA and surrounding carbon. Figure 5b shows the X-ray diffraction (XRD) patterns of Si-CNF composites, Micro-C/Si-CNF composites, and Meso-C/Si-CNF composites used to examine the crystal structures. The diffraction data of pure Si are exhibited for comparison. The diffraction peaks of all samples were observed at 28.5, 47.4, 56.2, 69.3, 76.6, and 88.3°, which correspond to (111), (220), (311), (400), (331), and (422) planes of crystalline Si, with the face-centered structure (JCPDS card no. 77-2111). This means that there was no crystallinity change of the Si nanoparticles during the pore-forming process.

To further investigate the chemical states, X-ray photoelectron spectroscopy (XPS) measurements were conducted (see Figure 6). High-resolution photoelectrons of Si 2p core-level peaks were observed at 99.6 and 103.2 eV, corresponding to Si and SiO_2 , respectively.^{3,4} Because of the stabilization process at 200 °C in air before carbonization, Si-CNF composites (Figure 6a) showed a large amount of SiO_2 phase (Si^{4+}). The stabilization process in air is a necessary condition to obtain high-quality carbon using dehydrogenation and cyclization of PAN.^{6,12,17,18} Therefore, the Si nanoparticles of Si-CNF composites are slightly oxidized on the surface because

of a thin carbon layer on the surface. As is widely known, SiO_2 shows poor capacities in LIBs due to its low electrical conductivity.^{3,4,16,19} Thus, antioxidation of the Si nanoparticles is crucial to obtain high capacities for LIBs. Micro-C/Si-CNF (Figure 6b) and Meso-C/Si-CNF composites (Figure 6c) exhibited a small amount of the SiO_2 phase (Si^{4+}), indicating that an extra carbon skin on the surface could efficiently prevent the oxidation of Si nanoparticles during the stabilization process in air, as shown in Figure S4. Therefore, introduction of an extra carbon skin on the Si-CNF composites could reduce the SiO_2 content from 49% (Si-CNF composites) to 8% (Micro-C/Si-CNF composites) and 9% (Meso-C/Si-CNF composites) (see Figure 6d).

To examine the electrochemical kinetics of the prepared electrodes, electrochemical impedance spectroscopy (EIS) measurements were conducted using fresh cells. Figure 7a shows Nyquist plots of the prepared electrodes at open-circuit potential. The semicircle in the high-frequency region is imputed to the charge-transfer resistance (R_{ct}) between the electrode and the electrolyte interface.^{6–8} The slant line in the low-frequency region is ascribed to the Li-ion diffusion performance in the electrode, referred to as the Warburg impedance.^{6–8} Meso-C/Si-CNF composites presented the lowest R_{ct} and the lowest Warburg impedance, manifesting enhanced charge-transfer kinetics and improved ionic diffusion related to a shorter Li-ion diffusion pathway. Therefore, the mesoporous carbon skin of Meso-C/Si-CNF composites could reduce the Warburg impedance, leading to an enhanced high-rate performance in LIBs. In addition, the Li-ion diffusion coefficient could be acquired from the low-frequency plots according to the following equation¹³

$$Z_{\text{real}} = R_e + R_{ct} + \sigma_w \omega^{-1/2} \quad (1)$$

$$D = R^2 T^2 / 2A^2 n^4 F^4 C_w^2 \sigma_w^2 \quad (2)$$

where σ_w is the Warburg impedance coefficient, D is the Li diffusion coefficient, R is the gas constant, T is the temperature, F is the Faraday constant, A is the area of the electrode, n is the number of electrons per molecule, and C is the molar concentration of Li ions. Figure S5 presents the relationship between Z_{real} and $f\omega^{-1/2}$ in the low-frequency region. The values of σ_w of Si, Si-CNF composites, Micro-C/Si-CNF composites, and Meso-C/Si-CNF composites are 26.5, 15.9, 13.4, and 8.5 $\Omega \text{ cm}^2 \text{ s}^{-1/2}$, respectively. The Li diffusion is reckoned by σ_w . The Li diffusion values of Si, Si-CNF composites, Micro-C/Si-CNF composites, and Meso-C/Si-CNF composites are 4.7×10^{-13} , 1.3×10^{-12} , 1.8×10^{-12} , and $4.5 \times 10^{-12} \text{ cm}^2 \text{ s}^{-1}$, respectively, indicating that mesoporous skin could efficiently improve the ionic diffusion performance during cycling owing to shorter Li-ion diffusion pathway. Figure 7b shows the Coulombic efficiency of electrodes at the current density of 100 mA g^{-1} over 100 cycles. Because of the development of solid electrolyte interface (SEI) layers on the electrode surface, all electrodes showed a low Coulombic efficiency during the first cycle. As is widely known, the SEI layers are commonly shaped owing to the reductive disintegration of electrolytes on an electrode surface, which leads to a high initial irreversible capacity. Nevertheless, the Meso-C/Si-CNF composites electrode exhibited the highest Coulombic efficiency of 67.7% compared to the Si (49.2%), Si-CNF composites (60.1%), and Micro-C/Si-CNF composites (65.5%) electrodes. This suggests that the well-dispersed Si nanoparticles can play a significant role in the enhancement of Coulombic efficiency during the first cycle.^{6,12,16} Moreover, the Coulombic efficiency of all electrodes reached almost 100% after five cycles, implying a highly reversible reaction. Figure 7c shows the discharge capacities with the cycling stabilities of the Si, Si-CNF composites, Micro-C/Si-CNF composites, and Meso-C/Si-CNF composites electrodes at the current density of 100 mA g^{-1} . For the Si electrode, a low specific discharge capacity of 59 mA h g^{-1} after 100 cycles with a poor cycling stability stayed uniformly between 30 and 100 cycles, suggesting a structural collapse of Si owing to the large volume expansion during cycling. The Si-CNF composites electrode indicated a low specific capacity of 414 mA h g^{-1} after 100 cycles with an insufficient cycling stability, indicating that the thin carbon layer of Si-CNF composites suffers from a large volume expansion of the Si nanoparticles. This result tends to be like those reported previously using Si and carbon composites without extra carbon skin.^{11,16} Thus, we introduced uniquely the extra carbon skin as the physical buffer layer and mesoporous carbon skin to achieve faster ionic diffusion. Especially, the extra carbon skin on the Si-CNF composites surface is essential to reconcile the volume expansion. The Micro-C/Si-CNF composites electrode presented a high specific discharge capacity of 1047 mA h g^{-1} after 100 cycles with an excellent cycling stability. These results demonstrate that improved electrochemical performance with capacity and cycling stability may be primarily ascribed to the efficient accommodation of the volume expansion for the Si nanoparticles using an extra carbon skin on the surface. Of note, the Meso-C/Si-CNF composites electrode showed a higher specific discharge capacity of 1140 mA h g^{-1} after 100 cycles with an outstanding cycling stability compared to other electrodes and previously reported results for carbon and Si composites-based electrodes, as shown in Table S2.^{22–39} To investigate the

structural and morphological variations of electrode materials after 100 cycles, the decomposed electrode materials were analyzed using the TEM measurement. The highly concentrated Si nanoparticles of Si-CNF composites (see Figure 7d) were detached from CNF due to a thin carbon layer on the surface. By contrast, the Si nanoparticles of Micro-C/Si-CNF composites (Figure 7e) and Meso-C/Si-CNF composites (Figure 7f) still encapsulated in CNF, suggesting that the extra carbon skin on the surface could accept a large volume expansion of the Si nanoparticles, leading to a high specific capacity and an excellent cycling stability for LIBs. Moreover, the charge–discharge curves of the Meso-C/Si-CNF composites electrode manifested typical electrochemical reactions of carbon and Si (see Figure 8). A low scan rate was applied to

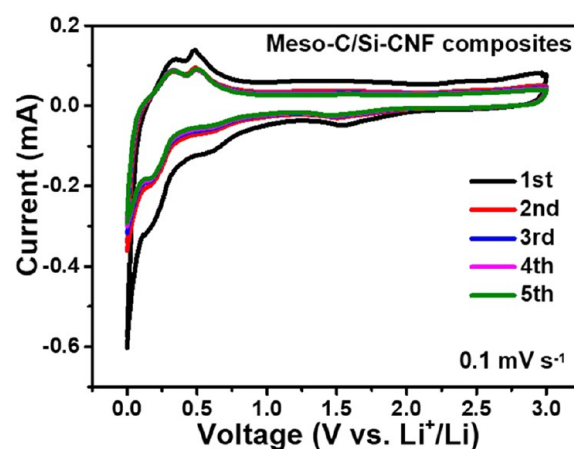


Figure 8. CV curves of Meso-C/Si-CNF composites electrode in the potential range of 0.05–3.00 V at a scan rate of 0.1 mV s^{-1} .

inquire the detailed electrochemical reaction during insertion/extraction of Li ions. In the first cathodic process, the reduction peak at around 0.8 V can be attributed to the irreversible formation of SEI layers on the surface.^{6,14} The reduction peaks at 0.4 and below 0.1 V are monitored related to the formation of Li–Si alloys.^{22,30,31,33} In the first anodic process, the oxidation peaks at 0.3 and 0.5 V are ascribed to the dealloying of Li–Si alloys.^{22,30,31,33} Also, cyclic voltammetry (CV) curves during the five cycles almost overlapped, implying the outstanding electrochemical reversibility. In addition, these results are in concurrence with the charge–discharge curves (Figure S6).

Because of the rapid development of the LIB industry and widening of its application areas, the high-rate performance and ultrafast cycling stability are substantial issues. Figure 9a shows the high-rate performance of electrodes at current densities of 100–2000 mA g^{-1} . The specific discharge capacities decreased owing to the reduced Li-ion diffusion time with increasing current densities during cycling. The Si-CNF composites electrode displayed a poor high-rate performance, similar to the one observed at a low-rate current density. Furthermore, the Micro-C/Si-CNF composites electrode also showed a relatively poor high-rate performance, indicating that a microspore structure on the skin had difficulties in accepting fast ions at a high-rate current density. To overcome these problems, we introduced the novel mesoporous carbon skin. Surprisingly, the Meso-C/Si-CNF composites electrode displayed a remarkable high-rate performance of 1230–969 mA h g^{-1} with current densities of 100 and 2000 mA g^{-1} . To

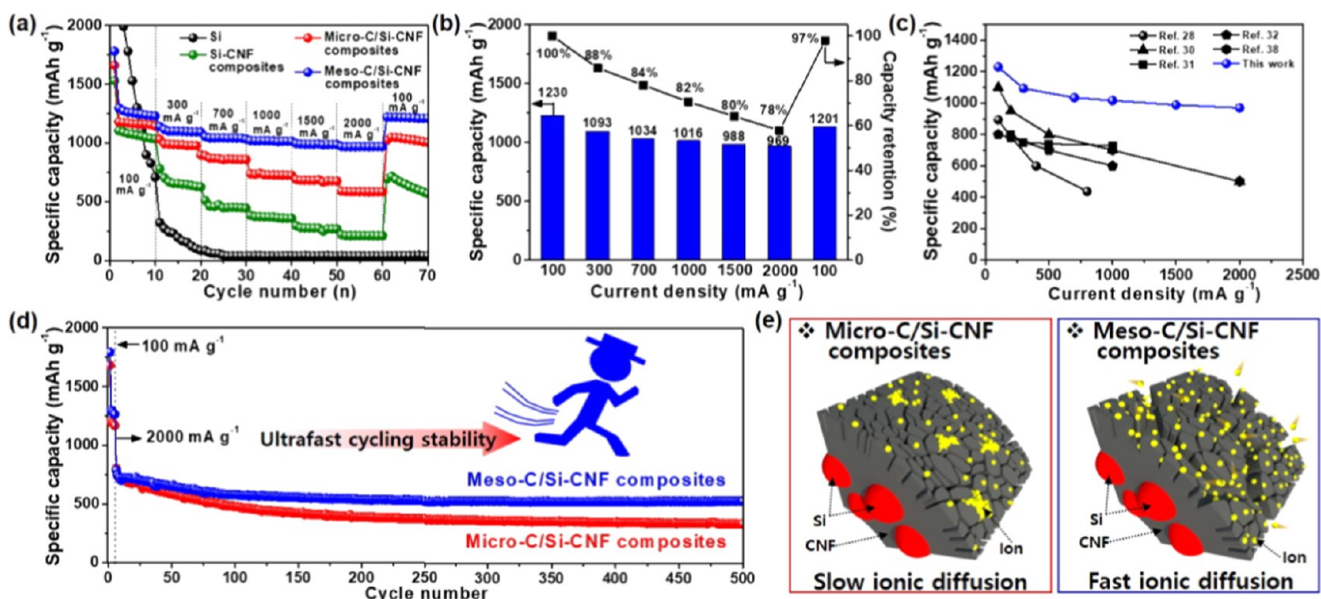


Figure 9. (a) High-rate performance at current densities of 100, 300, 700, 1000, 1500, and 2000 mA g⁻¹; (b) detailed specific capacities and capacity retentions of Meso-C/Si-CNF composites electrode with increasing current densities; (c) comparison of high-rate performance with the previously reported results for carbon and Si composite-based electrodes in LIBs; (d) ultrafast cycling stability at the current density of 2000 mA g⁻¹ over 500 cycles; (e) schematic illustration of the ionic diffusion process in Micro-C/Si-CNF composites and Meso-C/Si-CNF composites.

illustrate, the specific capacities and the capacity retentions at high-rate current densities of the Meso-C/Si-CNF composites electrode are summarized in Figure 9b. After high-rate tests, the Meso-C/Si-CNF composites electrode exhibited an outstanding capacity retention of 97% when the current density mended to 100 mA g⁻¹. This is the highest performance at high-rate current densities compared to previously that reported for carbon and Si composite-based electrodes (see Figure 9c).^{28,30–32,38} The improved high-rate performance of Meso-C/Si-CNF composites is ascribed to the increased mesopore volume at the carbon skin, leading to a shorter Li-ion diffusion pathway at high-rate current densities. In addition, the application of LIBs can potentially expand to the areas of ultrafast cycling at high current densities. Figure 9d shows the ultrafast cycling stability of the Micro-C/Si-CNF composites and Meso-C/Si-CNF composites electrodes at a high current density of 2000 mA g⁻¹ over 500 cycles. Compared to the Micro-C/Si-CNF composites electrode (159 mA h g⁻¹), the Meso-C/Si-CNF composites electrode displayed outstanding performance for ultrafast cycling stability with 532 mA h g⁻¹ after 500 cycles. The improved ultrafast cycling stability of the Meso-C/Si-CNF composites electrode is mainly attributed to the favorable ionic diffusion using a mesoporous carbon skin, suggesting that mesopores were more stable than micropores from faster ionic diffusion during cycling (see Figure 9e).

To test the influence of a mesoporous carbon skin on an ultrafast cycling stability at a high current density of 2000 mA g⁻¹, SEM and TEM analyses were performed using decomposed electrode materials (see Figure 10). Micro-C/Si-CNF composites (Figure 10a,c) showed the aggregated Si nanoparticles on the surface, implying that, because of the low ionic diffusion performance, the microporous structure on the carbon skin could not accommodate the rapid large volume expansion of the Si nanoparticles. On the other hand, the morphology and structure of Meso-C/Si-CNF composites (Figure 10b,d) were satisfactorily maintained after the ultrafast cycling test, which showed that the mesoporous carbon skin

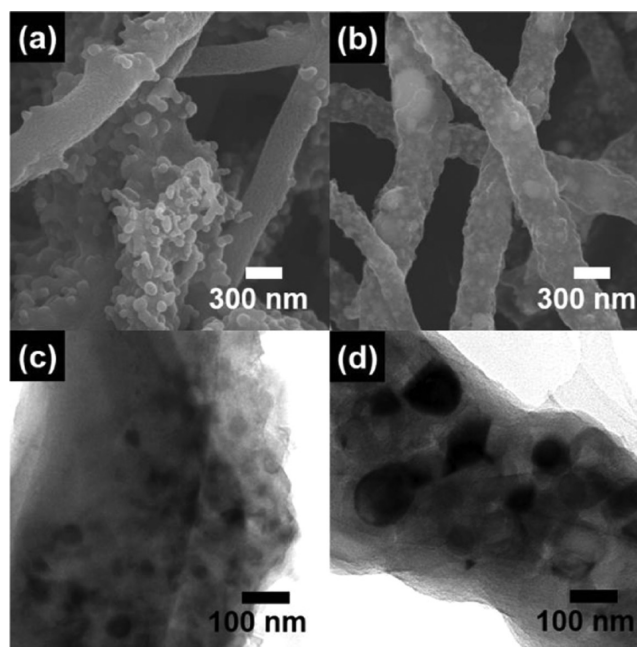


Figure 10. SEM images of (a) Micro-C/Si-CNF composites and (b) Meso-C/Si-CNF composites after 500 cycles at the current density of 2000 mA g⁻¹. TEM images of (c) Micro-C/Si-CNF composites and (d) Meso-C/Si-CNF composites after 500 cycles at the current density of 2000 mA g⁻¹.

with improved ionic diffusion performance is helpful in a rapid large volume expansion of the Si nanoparticles.

Therefore, in the present study, outstanding electrochemical properties of Meso-C/Si-CNF composites electrode were achieved by introducing a unique structure. The enhanced performance can be attributed to two effects. First, the introduction of an extra carbon skin on the surface enables an efficient accommodation of volume expansion of the Si nanoparticles, leading to enhanced capacities with a superb

cycling stability. Second, the mesoporous carbon skin could decrease the Li-ion diffusion pathway, leading to an improved ionic diffusion performance with the highest Li diffusion value of $4.5 \times 10^{-12} \text{ cm}^2 \text{ s}^{-1}$ among other electrodes. These results led to an outstanding high-rate performance at ultrahigh current density.

CONCLUSIONS

In the present study, Meso-C/Si-CNF composites as an anode material for LIBs were successfully synthesized by hydrothermal reaction, PMMA coating process, and carbonization process. Specifically, we proposed a unique concept of mesoporous carbon skin. The optimized Meso-C/Si-CNF composites indicated novel features for the high mesopore volume fraction of 47.9% with the mesopore sizes ranging from 2 to 3 nm. The remarkably enhanced electrochemical performances of Meso-C/Si-CNF composites electrode with a high specific discharge capacity with a superb cycling stability (1140 mA h g⁻¹ at 100 mA g⁻¹ after 100 cycles), an excellent high-rate performance (969 mA h g⁻¹ at 2000 mA g⁻¹), and an outstanding ultrafast cycling stability (532 mA h g⁻¹ at 2000 mA g⁻¹ after 500 cycles) were clearly demonstrated by the following factors: (1) the high specific discharge capacity with an excellent cycling stability is related to an extra carbon skin on the surface, which effectively accommodates the large volume expansions of the Si nanoparticles; (2) the improved high-rate performance and outstanding ultrafast cycling stability can be attributed to novel mesoporous skin, providing a shorter Li-ion diffusion pathway. Taken together, these findings indicate that the skin engineering of electrode materials based on a mesoporous structure might be a promising approach not only for fundamental studies related to an ionic diffusion, but also for the practical utilization of ultrafast energy-storage devices.

ASSOCIATED CONTENT

Supporting Information

The Supporting Information is available free of charge on the ACS Publications website at DOI: 10.1021/acsami.7b15950.

Experimental section, additional SEM and TEM images, particle size distribution of Si nanoparticles, DSC analysis, XPS images, relationship between Z_{real} and $\omega^{-1/2}$ in the low-frequency range, charge–discharge curves, BET results, and cycling stability comparison (PDF)

AUTHOR INFORMATION

Corresponding Author

*E-mail: hjahn@seoultech.ac.kr.

ORCID

Hyo-Jin Ahn: 0000-0002-5786-3937

Notes

The authors declare no competing financial interest.

ACKNOWLEDGMENTS

This research was supported by Basic Science Research Program through the National Research Foundation of Korea (NRF) funded by the Ministry of Science, ICT and Future Planning (NRF-2015R1A1A1A05001252).

REFERENCES

- (1) Armand, M.; Tarascon, J.-M. Building Better Batteries. *Nature* **2008**, *451*, 652–657.
- (2) Bruce, P. G.; Scrosati, B.; Tarascon, J.-M. Nanomaterials for Rechargeable Lithium Batteries. *Angew. Chem., Int. Ed.* **2008**, *47*, 2930–2946.
- (3) Cook, J. B.; Kim, H.-S.; Lin, T. C.; Robbenolt, S.; Detsi, E.; Dunn, B. S.; Tolbert, S. H. Tuning Porosity and Surface Area in Mesoporous Silicon for Application in Li-Ion Battery Electrodes. *ACS Appl. Mater. Interfaces* **2017**, *9*, 19063–19073.
- (4) Lu, B.; Ma, B.; Deng, X.; Li, W.; Wu, Z.; Shu, H.; Wang, X. Cornlike Ordered Mesoporous Silicon Particles Modified by Nitrogen-Doped Carbon Layer for the Application of Li-Ion Battery. *ACS Appl. Mater. Interfaces* **2017**, *9*, 32829–32839.
- (5) Jiang, Y.; Guo, Y.; Lu, W.; Feng, Z.; Xi, B.; Kai, S.; Zhang, J.; Feng, J.; Xiong, S. Rationally Incorporated MoS₂/SnS₂ Nanoparticles on Graphene Sheets for Lithium-Ion and Sodium-Ion Batteries. *ACS Appl. Mater. Interfaces* **2017**, *9*, 27697–27706.
- (6) An, G.-H.; Lee, D.-Y.; Ahn, H.-J. Tunneled Mesoporous Carbon Nanofibers with Embedded ZnO Nanoparticles for Ultrafast Lithium Storage. *ACS Appl. Mater. Interfaces* **2017**, *9*, 12478–12485.
- (7) An, G.-H.; Lee, D.-Y.; Ahn, H.-J. Carbon-Encapsulated Hollow Porous Vanadium-Oxide Nanofibers for Improved Lithium Storage Properties. *ACS Appl. Mater. Interfaces* **2016**, *8*, 19466–19474.
- (8) Lee, Y.-W.; An, G.-H.; Kim, B.-S.; Hong, J.; Pak, S.; Lee, E.-H.; Cho, Y.; Lee, J.; Giraud, P.; Cha, S. N.; Ahn, H.-J.; Sohn, J. I.; Kim, J. M. Synergistic Effects of a Multifunctional Graphene Based Interlayer on Electrochemical Behavior and Structural Stability. *ACS Appl. Mater. Interfaces* **2016**, *8*, 17651–17658.
- (9) Xing, Y.; Wang, Y.; Zhou, C.; Zhang, S.; Fang, B. Simple Synthesis of Mesoporous Carbon Nanofibers with Hierarchical Nanostructure for Ultrahigh Lithium Storage. *ACS Appl. Mater. Interfaces* **2014**, *6*, 2561–2567.
- (10) An, G.-H.; Lee, D.-Y.; Ahn, H.-J. Tofu-Derived Carbon Framework with Embedded Ultrasmall Tin Nanocrystals for High-Performance Energy Storage Devices. *J. Alloys Compd.* **2017**, *722*, 60–68.
- (11) Wang, Y.; Wen, X.; Chen, J.; Wang, S. Foamed Mesoporous Carbon/Silicon Composite Nanofiber Anode for Lithium Ion Batteries. *J. Power Sources* **2015**, *281*, 285–292.
- (12) An, G.-H.; Lee, D.-Y.; Lee, Y.-J.; Ahn, H.-J. Ultrafast Lithium Storage Using Antimony-Doped Tin Oxide Nanoparticles Sandwiched between Carbon Nanofibers and a Carbon Skin. *ACS Appl. Mater. Interfaces* **2016**, *8*, 30264–30270.
- (13) Lee, Y.-W.; Kim, D.-M.; Kim, S.-J.; Kim, M.-C.; Choe, H.-S.; Lee, K.-H.; Sohn, J. I.; Cha, S. N.; Kim, J. M.; Park, K.-W. In Situ Synthesis and Characterization of Ge Embedded Electrospun Carbon Nanostructures as High Performance Anode Material for Lithium-Ion Batteries. *ACS Appl. Mater. Interfaces* **2016**, *8*, 7022–7029.
- (14) An, G.-H.; Sohn, J. I.; Ahn, H.-J. Hierarchical Architecture of Hybrid Carbon Encapsulated Hollow Manganese Oxide Nanotubes with a Porous-Wall Structure for High-Performance Electrochemical Energy Storage. *J. Mater. Chem. A* **2016**, *4*, 2049–2054.
- (15) Li, H.; Wang, Z.; Chen, L.; Huang, X. Research on Advanced Materials for Li-ion Batteries. *Adv. Mater.* **2009**, *21*, 4593–4607.
- (16) An, G.-H.; Ahn, H.-J. Ultrafast Lithium Storage of High Dispersed Silicon and Titanium Oxide Nanoparticles in Carbon. *J. Alloys Compd.* **2017**, *710*, 274–280.
- (17) An, G.-H.; Ahn, H.-J. Carbon Nanofiber/Cobalt Oxide Nanopyramid Core-shell Nanowires for High-Performance Lithium-Ion Batteries. *J. Power Sources* **2014**, *272*, 828–836.
- (18) An, G.-H.; Lee, D.-Y.; Ahn, H.-J. Vanadium Nitride Encapsulated Carbon Fibre Networks with Furrowed Porous Surfaces for Ultrafast Asymmetric Supercapacitors with Robust Cycle Life. *J. Mater. Chem. A* **2017**, *5*, 19714–19720.
- (19) Wu, J.; Zhu, Z.; Zhang, H.; Fu, H.; Li, H.; Wang, A.; Zhang, H.; Hu, Z. A Novel Nano-Structured Interpenetrating Phase Composite of Silicon/Graphite-Tin for Lithium-Ion Rechargeable Batteries Anode Materials. *J. Alloys Compd.* **2014**, *596*, 86–91.

- (20) An, G.-H.; Koo, B.-R.; Ahn, H.-J. Activated Mesoporous Carbon Nanofibers Fabricated using Water Etching-Assisted Templating for High-Performance Electrochemical Capacitors. *Phys. Chem. Chem. Phys.* **2016**, *18*, 6587–6594.
- (21) An, G.-H.; Ahn, H.-J. Activated Porous Carbon Nanofibers using Sn Segregation for High-Performance Electrochemical Capacitors. *Carbon* **2013**, *65*, 87–96.
- (22) Lee, B.-S.; Son, S.-B.; Park, K.-M.; Seo, J.-H.; Lee, S.-H.; Choi, I.-S.; Oh, K.-H.; Yu, W.-R. Fabrication of Si Core/C Shell Nanofibers and Their Electrochemical Performances as a Lithium-Ion Battery Anode. *J. Power Sources* **2012**, *206*, 267–273.
- (23) Fu, K.; Lu, Y.; Dirican, M.; Chen, C.; Yanilmaz, M.; Shi, Q.; Bradford, P. D.; Zhang, X. Chamber-Confined Silicon–Carbon Nanofiber Composites for Prolonged Cycling Life of Li-Ion Batteries. *Nanoscale* **2014**, *6*, 7489–7495.
- (24) Hieu, N. T.; Suk, J.; Kim, D. W.; Chung, O. H.; Park, J. S.; Kang, Y. Silicon Nanoparticle and Carbon Nanotube Loaded Carbon Nanofibers for Use in Lithium-Ion Battery Anodes. *Synth. Met.* **2014**, *198*, 36–40.
- (25) Li, Y.; Guo, B.; Ji, L.; Lin, Z.; Xu, G.; Liang, Y.; Zhang, S.; Toprakci, O.; Hu, Y.; Alcoutlabi, M.; Zhang, X. Structure Control and Performance Improvement of Carbon Nanofibers Containing a Dispersion of Silicon Nanoparticles Nanofibers Containing a Dispersion of Silicon Nanoparticles. *Carbon* **2013**, *51*, 185–194.
- (26) Xue, L.; Fu, K.; Li, Y.; Xu, G.; Lu, Y.; Zhang, S.; Toprakci, O.; Zhang, X. Si/C Composite Nanofibers with Stable Electric Conductive Network for Use as Durable Lithium-Ion Battery Anode. *Nano Energy* **2013**, *2*, 361–367.
- (27) Ji, L.; Zhang, X. Evaluation of Si/Carbon Composite Nanofiber-Based Insertion Anodes for New-Generation Rechargeable Lithium-Ion Batteries. *Energy Environ. Sci.* **2010**, *3*, 124–129.
- (28) Dirican, M.; Yildiz, O.; Lu, Y.; Fang, X.; Jiang, H.; Kizil, H.; Zhang, X. Flexible Binder-Free Silicon/Silica/Carbon Nanofiber Composites as Anode for Lithium-Ion Batteries. *Electrochim. Acta* **2015**, *169*, 52–60.
- (29) Li, Y.; Sun, Y.; Xu, G.; Lu, Y.; Zhang, S.; Xue, L.; Jur, J. S.; Zhang, X. Tuning Electrochemical Performance of Si-Based Anodes for Lithium-Ion Batteries by Employing Atomic Layer Deposition Alumina Coating. *J. Mater. Chem. A* **2014**, *2*, 11417–11425.
- (30) Liu, Y.; Huang, K.; Fan, Y.; Zhang, Q.; Sun, F.; Gao, T.; Wang, Z.; Zhong, J. Binder-Free Si Nanoparticles@Carbon Nanofiber Fabric as Energy Storage Material. *Electrochim. Acta* **2013**, *102*, 246–251.
- (31) Wang, M.-S.; Song, W.-L.; Wang, J.; Fan, L.-Z. Highly Uniform Silicon Nanoparticle/Porous Carbon Nanofiber Hybrids Towards Free-Standing High-Performance Anodes for Lithium-Ion Batteries. *Carbon* **2015**, *82*, 337–345.
- (32) Xu, Z.-L.; Zhang, B.; Kim, J.-K. Electrospun Carbon Nanofiber Anodes Containing Monodispersed Si Nanoparticles and Graphene Oxide with Exceptional High Rate Capacities. *Nano Energy* **2014**, *6*, 27–35.
- (33) Fan, X.; Zou, L.; Zheng, Y.-P.; Kang, F.-Y.; Shen, W.-C. Electrospinning Preparation of Nanosilicon/Disordered Carbon Composite as Anode Materials in Li-Ion Battery. *Electrochim. Solid-State Lett.* **2009**, *12*, A199–A201.
- (34) Lee, B.-S.; Son, S.-B.; Seo, J.-H.; Park, K.-M.; Lee, G.; Lee, S.-H.; Oh, K. H.; Ahn, J.-P.; Yu, W.-R. Facile Conductive Bridges Formed Between Silicon Nanoparticles Inside Hollow Carbon Nanofibers. *Nanoscale* **2013**, *5*, 4790–4796.
- (35) Lee, B.-S.; Yang, H.-S.; Jung, H.; Jeon, S.-Y.; Jung, C.; Kim, S.-W.; Bae, J.; Choong, C.-L.; Im, J.; Chung, U.-I.; Park, J.-J.; Yu, W.-R. Novel Multi-Layered 1-D Nanostructure Exhibiting the Theoretical Capacity of Silicon for a Super Enhanced Lithium-Ion Battery. *Nanoscale* **2014**, *6*, 5989–5998.
- (36) Zhang, Y.-C.; You, Y.; Xin, S.; Yin, Y.-X.; Zhang, J.; Wang, P.; Zheng, X.-s.; Cao, F.-F.; Guo, Y.-G. Rice Husk-Derived Hierarchical Silicon/Nitrogen-Doped Carbon/Carbon Nanotube Spheres as Low-Cost and High-Capacity Anodes for Lithium-Ion Batteries. *Nano Energy* **2016**, *25*, 120–127.
- (37) Shin, J.; Park, K.; Ryu, W.-H.; Jung, J.-W.; Kim, I.-D. Graphene Wrapping as a Protective Clamping Layer Anchored to Carbon Nanofibers Encapsulating Si Nanoparticles for a Li-Ion Battery Anode. *Nanoscale* **2014**, *6*, 12718–12726.
- (38) Chen, Y.; Hu, Y.; Shao, J.; Shen, Z.; Chen, R.; Zhang, X.; He, X.; Song, Y.; Xing, X. Pyrolytic Carbon-Coated Silicon/Carbon Nanofiber Composite Anodes for High-Performance Lithium-Ion Batteries. *J. Power Sources* **2015**, *298*, 130–137.
- (39) Yang, J.; Wang, Y.-X.; Chou, S.-L.; Zhang, R.; Xu, Y.; Fan, J.; Zhang, W.-x.; Liu, H. K.; Zhao, D.; Dou, S. X. Yolk-Shell Silicon-Mesoporous Carbon Anode with Compact Solid Electrolyte Interphase Film for Superior Lithium-Ion Batteries. *Nano Energy* **2015**, *18*, 133–142.